Research Square

Preprints are preliminary reports that have not undergone peer review.
They should not be considered conclusive, used to inform clinical practice,
or referenced by the media as validated information.

Numerical Investigation of Rectangular Cutout Size Effects on Thermal- Hydraulic Performance in a Circular Tube with Twisted Tape Inserts and Al_2O_3 Nanofluid

Sajid Akram Bhuiyan
Chittagong University of Engineering & Technology (CUET)
MM Roshid
Chittagong University of Engineering & Technology (CUET)
Mohammad Fahim Ahmed
fahimniloy2314@gmail.com
Chittagong University of Engineering & Technology (CUET)
Md. Suez
Chittagong University of Engineering & Technology (CUET)

Research Article

Keywords: Perforated twisted tape, Al2O3 nanofluid, Heat transfer enhancement, Friction factor, Thermal enhancement efficiency, CFD

Posted Date: November 20th, 2026

DOI: https://doi.org/10.21203/rs.3.rs-11788081/v1

License: This work is licensed under a Creative Commons Attribution 4.0 International License.
Read Full License

Additional Declarations: No competing interests reported.

Numerical Investigation of Rectangular Cutout Size Effects on Thermal-Hydraulic Performance in a Circular Tube with Twisted Tape Inserts and Al_2O_3 Nanofluid

Sajid Akram Bhuiyan[a], MM Roshid[a], Mohammad Fahim Ahmed[a,*], Md. Suez[a]

[a] *Department of Mechanical Engineering, Chittagong University of Engineering & Technology (CUET), Chattogram-4349, Bangladesh*

*Corresponding author: Mohammad Fahim Ahmed | fahimniloy2314@gmail.com

ABSTRACT

Twisted tape inserts are a well-established passive technique that promotes swirl flow and disrupts the thermal boundary layer, and perforating the tape further modifies the induced turbulence. In this work, the thermal-hydraulic performance of rectangular-cut perforated twisted tape (PTT) inserts combined with Al_2O_3 nanofluid is numerically investigated in a circular tube using ANSYS Fluent. Three perforation geometries, PTT-01 (20 mm × 30 mm), PTT-02 (10 mm × 20 mm), and PTT-03 (5 mm × 15 mm), were examined together with three Al_2O_3 volume fractions (0.05%, 0.15%, 0.30%) over Reynolds numbers of 5000–20,000 under constant wall heat flux. The plain-tube results were validated against the Gnielinski and Petukhov correlations before the insert configurations were evaluated. All PTT geometries enhanced the Nusselt number relative to the plain tube, with PTT-02 producing the strongest heat transfer augmentation (Nusselt number ratio of 1.52 at Re = 20,000) but also the largest friction factor penalty. When the combined benefit was assessed through the thermal enhancement efficiency, PTT-01 with 0.05% Al_2O_3 nanofluid gave the best overall thermal-hydraulic balance, with an efficiency of 0.848. The influence of nanoparticle loading on performance was comparatively small over the concentration range tested. These results indicate that rectangular-cut PTT inserts are an effective passive enhancement technique, but that insert geometry, not nanofluid concentration, is the dominant design variable, and an optimum insert must be selected by weighing heat transfer gain against pressure penalty rather than by maximizing Nusselt number alone.

Keywords: *Perforated twisted tape; Al_2O_3 nanofluid; Heat transfer enhancement; Friction factor; Thermal enhancement efficiency; CFD*

Nomenclature

Symbol	Definition	Symbol	Definition
A_s	heated surface area (m^2)	d	tube diameter (m)
C_p	specific heat ($J\ kg^{-1}\ K^{-1}$)	f	Darcy friction factor
h	heat-transfer coefficient ($W\ m^{-2}\ K^{-1}$)	k	thermal conductivity ($W\ m^{-1}\ K^{-1}$)
L	tube length (m)	Nu	Nusselt number
Pr	Prandtl number	Q	heat-transfer rate (W)
Re	Reynolds number	T	temperature (K)
u, v	velocity ($m\ s^{-1}$)	ΔP	pressure drop (Pa)
η, PEC	performance evaluation criterion	φ	particle volume fraction
ρ	density ($kg\ m^{-3}$)	μ	dynamic viscosity (Pa s)
bf	base fluid	nf	nanofluid
np	nanoparticle	0	plain-tube reference

1 Introduction

Escalating energy demand and the need to reduce industrial energy consumption have intensified efforts to improve the effectiveness of thermal system[1–3].Heat exchangers are indispensable in HVAC and refrigeration systems, power generation facilities, chemical and process industries, heat-recovery units, and numerous heating and cooling operations [1,2,4,5]. Improving their performance can reduce exchanger size, material consumption, operating cost, and energy losses while supporting more compact thermal equipment [1,2,4,6]. Accordingly, heat transfer enhancement must increase thermal duty without imposing an unacceptable pressure drop or pumping-power penalty [2–5,7].

Heat transfer augmentation methods are generally classified as active, passive, or compound approaches [1–4]. Active techniques employ external power or controlled excitation, whereas passive techniques modify the surface, working fluid, or flow path without requiring additional external energy input [1–4]. Passive methods are therefore attractive because of their relative simplicity, ease of installation, and suitability for upgrading existing exchangers, although the resulting flow resistance must still be considered [4–6,8]. Representative passive approaches include roughened or extended surfaces, corrugated passages, swirl-generating inserts, and nanofluids, with combinations of these methods forming compound enhancement systems [1–3,6]. Among insert based techniques, twisted tapes are extensively adopted because they provide a simple and economical means of producing rotational flow and strengthening radial mixing [2–6].

The limited thermal conductivity of conventional liquids such as water restricts their capacity to remove or transport heat effectively in compact exchangers [8–10]. Nanofluids are engineered suspensions of nanoscale solid particles in a base liquid; the dispersed particles modify the effective thermal conductivity and other thermophysical properties of the working medium, thereby influencing convective transport [8–11]. Al_2O_3/water nanofluid has received considerable attention because alumina nanoparticles can enhance thermal conductivity and heat-transfer coefficients while remaining applicable at relatively low particle concentrations[8–10]. Its performance nevertheless depends on dispersion stability, viscosity, particle agglomeration, and the associated hydraulic penalty [8,10,11]. Increasing particle volume fraction generally increases thermal conductivity and Nusselt number, but it may also raise viscosity, friction factor, and

pressure drop; consequently, concentration must be selected using a thermo-hydraulic rather than a purely thermal criterion [8–12].

Twisted-tape inserts enhance convection by generating swirl, increasing wall core fluid exchange, extending the flow path, and repeatedly disturbing the thermal boundary layer [4–6,8]. Their performance is strongly governed by twist ratio, pitch distribution, tape width and thickness, and geometrical modifications such as holes, dimples, notches, wings, and V- or rectangular cuts [4–6,11,13,14]. Perforations and cuts can create local jets, secondary vortices, and additional turbulence while also changing flow blockage and frictional losses; hence, the selected geometry determines the balance between Nusselt number enhancement and pressure drop penalty[4,5,13,14]. Numerical comparisons of plain, perforated, and dimpled tapes and investigations of porous or large-hole tapes confirm that modified inserts can outperform conventional tapes, although the configuration producing the greatest heat transfer does not necessarily deliver the best overall performance [3–5,14]. The compound application of nanofluids and twisted tapes can provide further enhancement, as demonstrated for Al_2O_3/water with conventional, progression ratio, finned, V-cut, and variable pitch tapes [8–11].

The literature therefore establishes the individual and combined potential of nanofluids and twisted tapes, but the configurations investigated have predominantly involved conventional tapes, V-cuts, variable pitches, circular fins, holes, or dimples [4,8–11,14]. Despite extensive research, limited attention has been devoted to the numerical thermo-hydraulic behaviour of Al_2O_3/water nanofluid used specifically with a customized rectangular-cut perforated twisted tape, particularly regarding the simultaneous effects on flow structure, heat transfer, friction, and net performance [4,8–11]. Because opening geometry governs jet formation and secondary-flow development, the performance of rectangular cuts cannot be reliably inferred from results obtained using circular holes, dimples, or V-cuts and therefore requires configuration specific assessment [4,5,13,14]. The anticipated coupled enhancement mechanism and its associated hydraulic trade-off are illustrated conceptually in Fig. 1.

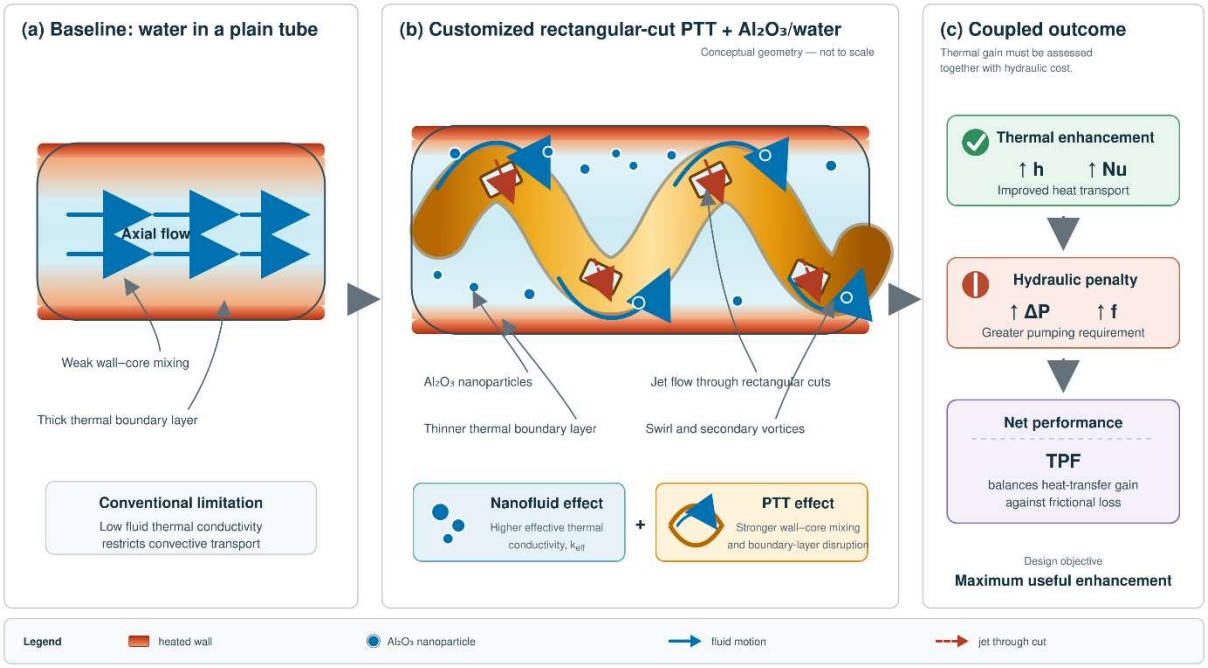


Fig. 1 Conceptual comparison of the baseline and enhanced configurations, illustrating the heat-transfer mechanisms and associated hydraulic trade-off for Al_2O_3/water nanofluid flowing through a heated tube equipped with a customized rectangular-cut perforated twisted-tape insert

Therefore, the present study aims to:

1. Develop a three dimensional numerical model of Al_2O_3/water nanofluid flow through a heat exchanger tube fitted with a customized rectangular cut perforated twisted tape insert.
2. Investigate the effects of Reynolds number and nanoparticle volume fraction on the temperature, velocity, and secondary flow fields.
3. Quantify the heat transfer coefficient, Nusselt number, pressure drop, and friction factor, and compare these parameters with those of a plain tube.
4. Evaluate the overall thermohydraulic performance using the thermal performance factor.
5. Identify the physical mechanisms governing the interaction between nanofluid transport and the swirl and jet flows induced by the twisted tape insert.

The remainder of this manuscript presents the computational geometry and numerical methodology, model validation, results and discussion, and principal conclusions. The key novelty of this study lies in the integrated numerical assessment of Al_2O_3/water nanofluid flow with a customized rectangular cut perforated twisted tape insert, considering both heat transfer enhancement and hydraulic losses.

2 Numerical methodology

2.1 Physical model and geometry

The computational domain consists of a circular brass tube of length 1000 mm and outer diameter 70 mm, fitted with a single stainless steel twisted tape insert of length 1000 mm, height 65 mm, thickness 1 mm, and 12 turns. The tape is perforated with rectangular cuts distributed along its length; three perforation sizes were examined PTT-01 (20 mm × 30 mm), PTT-02 (10 mm × 20 mm), and PTT-03 (5 mm × 15 mm) each

tape containing 48 rectangular cuts in total. The tube and tape geometry are shown in Figs. 1 and 2, and the model dimensions are summarized in Table 1.

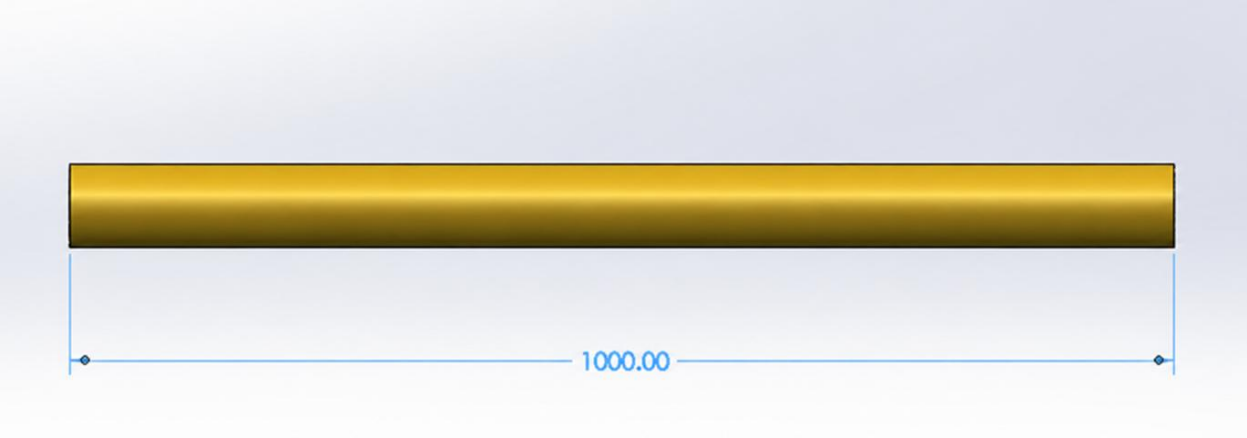


Fig. 2 Side view of the circular tube fitted with the perforated twisted tape insert

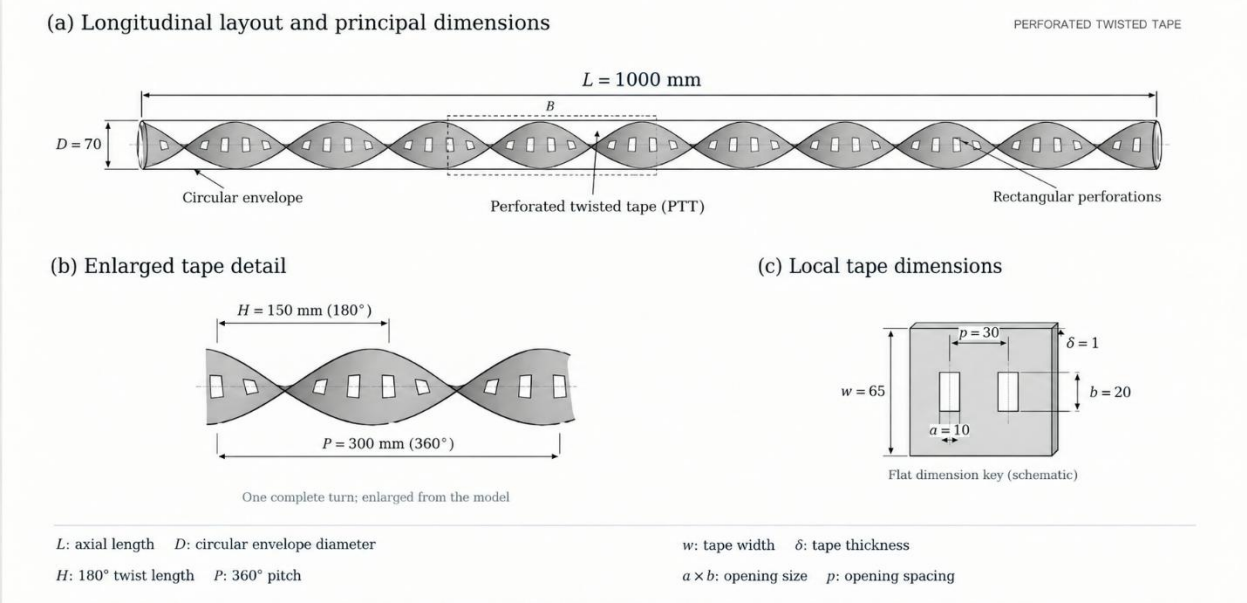


Fig. 3 Schematic of a circular tube with a rectangular-perforated twisted tape insert: (a) overall geometry and principal dimensions, (b) enlarged tape detail, and (c) local tape dimensions



Fig. 4 Dimension and position of the rectangular perforation on the twisted tape

Table 1. Dimensions of the computational model.

No.	Dimension	Value
1	Tube length	1000 mm
2	Tube outer diameter	70 mm
3	Twisted tape length	1000 mm
4	Twisted tape height	65 mm
5	Twisted tape thickness	1 mm
6	Number of turns	12
7	Number of twisted tapes	1
8	Rectangular cut length	15 mm
9	Rectangular cut width	5 mm
10	Total number of rectangular cuts	48

2.2 Governing equations

Steady, incompressible, three-dimensional turbulent flow was solved using the RNG k–ε turbulence model with standard wall functions. The governing continuity, momentum, and energy equations are:

$$\frac{\partial \rho}{\partial t} + \nabla \cdot (\rho u) = 0 \tag{1}$$

$$\frac{\partial (\rho u_i)}{\partial t} + \nabla \cdot (\rho u_i u) = -\frac{\partial p}{\partial x_i} + \nabla \cdot (\mu \nabla u_i) \tag{2}$$

$$\frac{\partial (\rho T)}{\partial t} + \nabla \cdot (\rho u T) = -p \nabla \cdot u + \nabla \cdot (k \nabla T) + \Phi + S_i \tag{3}$$

where ρ, u, p, μ, T, and k are the fluid density, velocity vector, pressure, dynamic viscosity, temperature, and thermal conductivity, respectively, and Φ and S_i are the viscous dissipation and energy source terms. Radiative heat transfer was neglected; heat transfer proceeded solely by forced convection.

2.3 Material and nanofluid properties

The tube was modelled as brass and the twisted tape as stainless steel; their thermophysical properties are given in Table 2. Water-based Al_2O_3 nanofluid was used as the working fluid at three particle volume fractions (φ = 0.05%, 0.15%, 0.30%). The base fluid and nanoparticle properties are listed in Table 3, and the effective nanofluid properties were computed from the standard mixture relations:

$$\rho_{nf} = (1 - \phi)\rho_{bf} + \phi \rho_{np} \tag{4}$$

$$(C_p)_{nf} = \frac{(1-\phi)\rho_{bf}(C_p)_{bf} + \phi \rho_{np}(C_p)_{np}}{\rho_{nf}} \tag{5}$$

$$k_{nf} = k_{bf} \cdot \frac{k_{np} + (n-1)k_{bf} - \phi(n-1)(k_{bf} - k_{np})}{k_{np} + (n-1)k_{bf} + \phi(k_{bf} - k_{np})} \tag{6}$$

$$\mu_{nf} = \frac{\mu_{bf}}{(1-\phi)^{2.5}} \tag{7}$$

Table 2. Material properties of the tube and twisted tape

Material	Density (kg/m³)	Specific heat (J/kg·K)	Thermal conductivity (W/m·K)
Brass	8711.6	382.32	192
Stainless steel	7916.4	456.47	15.365

Table 3. Base fluid and Al_2O_3 nanoparticle properties used to compute nanofluid properties.

Fluid / particle	Density (kg/m³)	Specific heat (J/kg·K)	Thermal conductivity (W/m·K)
Water (base fluid)	998.2	4182	0.6
Al_2O_3	3970	765	40

2.4 Mesh generation and grid independence

The geometry was modelled in SolidWorks 2021 and discretized using ANSYS Meshing. Body sizing controls were applied to achieve both global and local mesh refinement, with particular attention given to the perforated twisted tape and the regions surrounding the rectangular openings, where large velocity and thermal gradients were expected. Inflation layers were also generated adjacent to the tube wall to provide improved resolution of the near-wall boundary layer, as summarized in Table 4. A grid independence study was performed at Re=5000 using a reduced tube length of 500 mm for the PTT-01 configuration. The surface-averaged heat transfer coefficient and outlet temperature were monitored as the principal convergence parameters. The variation in these parameters became negligible when the mesh size exceeded approximately 2.25 million elements, and this mesh density was therefore adopted for all subsequent simulations (Fig. 3). Representative meshes of the perforated twisted tape are presented in Fig. 4, including the overall surface mesh and an enlarged view of the locally refined mesh surrounding the rectangular perforations.

Table 4. Body sizing parameters used for ANSYS meshing.

Mesh control	Element size (mm)	Defeature size (mm)	Curvature size (mm)	Proximity size (mm)
Body sizing 01	10	1	1	0.5
Body sizing 02	2	1	1	0.5

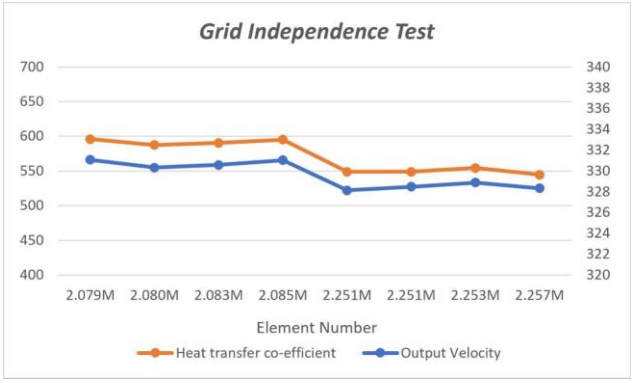


Fig. 5 Grid independence test for the numerical simulation (PTT-01, Re = 5000)

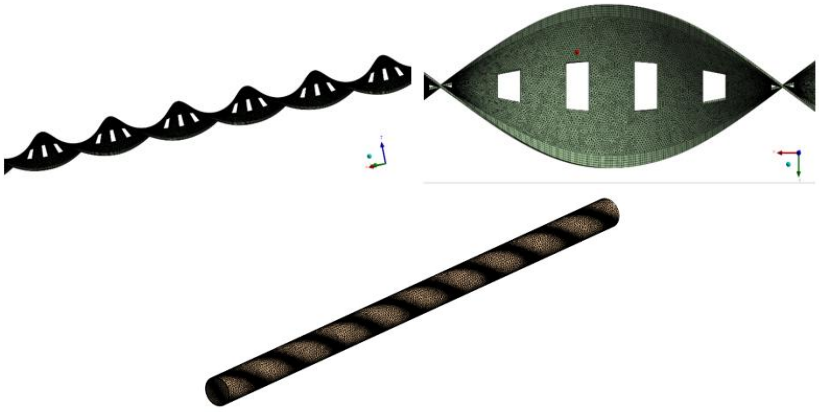


Fig. 6 Geometry and representative mesh of the perforated twisted tape insert, showing the overall configuration and locally refined regions around the rectangular perforations

2.5 Boundary conditions and solution method

A uniform velocity inlet corresponding to the target Reynolds number was specified, with an outflow condition at the exit and no slip walls. A constant wall temperature was applied to the outer tube wall; the interior tape fluid interfaces were coupled to correctly resolve conjugate heat transfer. The energy equation was solved together with the RNG k–ε turbulence closure; multiphase, radiation, species transport, and other physics models were disabled. The pressure velocity coupling used the SIMPLE scheme with second-order upwind discretization for momentum and energy, and simulations were run to convergence of the scaled residuals for each of the four target Reynolds numbers (5000, 10000, 15000, 20000) and three nanofluid concentrations for each of the three PTT geometries.

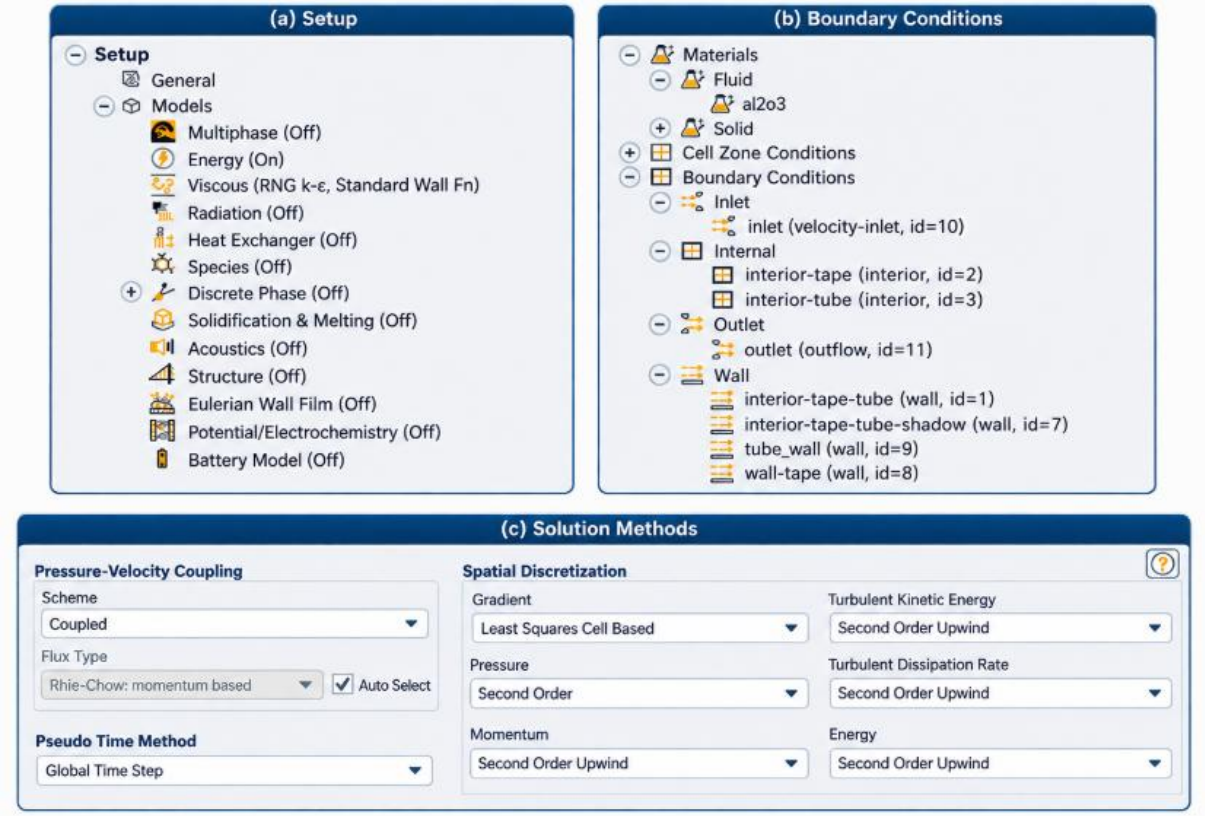


Fig. 7 Numerical simulation setup and solution methodology

2.6 Data reduction

The Reynolds number, Prandtl number, heat transfer coefficient, Nusselt number, and friction factor were computed from the simulation outputs as:

$$Re = \frac{\rho v d}{\mu}, \qquad Pr = \frac{\mu C_p}{k} \tag{8}$$

$$h = \frac{Q}{A_s(T_w - T_b)}, \qquad Nu = \frac{hd}{k} \tag{9}$$

$$f = \frac{\Delta P}{(L/d)(\rho v^2/2)} \tag{10}$$

The overall thermal-hydraulic performance of each twisted-tape configuration was evaluated using the performance evaluation criterion (PEC):

$$PEC = \frac{Nu/Nu_0}{(f/f_0)^{1/3}} \tag{11}$$

where the subscript 0 denotes the plain-tube reference at the same Reynolds number. $\eta > 1$ indicates that the heat transfer gain outweighs the frictional penalty; $\eta < 1$ indicates the opposite. Plain tube results were validated against the Gnielinski correlation for Nusselt number and the Petukhov correlation for friction factor:

$$Nu = \frac{(f/8)(Re-1000)Pr}{1+12.7(f/8)^{0.5}\left(Pr^{2/3}-1\right)} \tag{12}$$

$$f = (0.79 \ln Re - 1.64)^{-2} \tag{13}$$

3 Results and discussion

3.1 Validation of plain-tube results

The plain-tube simulation results were first validated against the Gnielinski and Petukhov correlations to establish confidence in the numerical model before evaluating the PTT inserts. Table 5 gives the simulated heat transfer coefficient, Nusselt number, and friction factor for the plain tube at Re = 5000–20,000, and Table 6 compares the correlation-based Nusselt number and friction factor with the simulation. The Nusselt number increased from 45.1538 at Re = 5000 to 155.124 at Re = 20,000, while the heat transfer coefficient rose from 387.03 to 1329.63 W/m²·K over the same range; the friction factor correspondingly decreased from 0.0501 to 0.03273 consistent with the expected reduction in relative flow resistance at higher Reynolds number. Figs. 8 and 9 show that the simulated Nusselt number and friction factor follow the same trend as the Gnielinski and Petukhov predictions across the full Reynolds number range, confirming that the numerical model is suitable for the subsequent insert simulations.

Table 5. Simulated heat transfer coefficient, Nusselt number, and friction factor for the plain tube.

Reynolds Number	Velocity m/s	Wall Temperature k	Bulk Temperature k	Heat Transfer Coefficient	Nusselt Number	Pressure Inlet	Friction Factor
5000	0.071772	498	314.378	387.0323	45.1538	2.7695	0.05019
10000	0.143544	498	312.277	738.5313	86.1620	7.4831	0.04071
15000	0.215316	498	310.622	1030.1386	120.182	17.8301	0.03592
20000	0.287088	498	309.94	1329.6348	155.124	28.8739	0.03273

Table 6. Validation of the plain-tube results against the Petukhov and Gnielinski correlations.

Re	f (Petukhov)	Nu (Gnielinski)
5000	0.0386	40.37
10000	0.0315	79.45
15000	0.0282	114.85
20000	0.0262	148.26

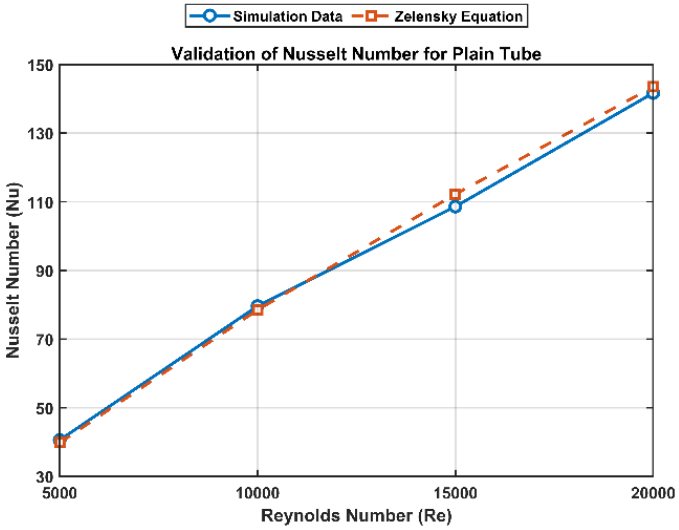


Fig. 8 Validation of the plain-tube Nusselt number against the Gnielinski correlation

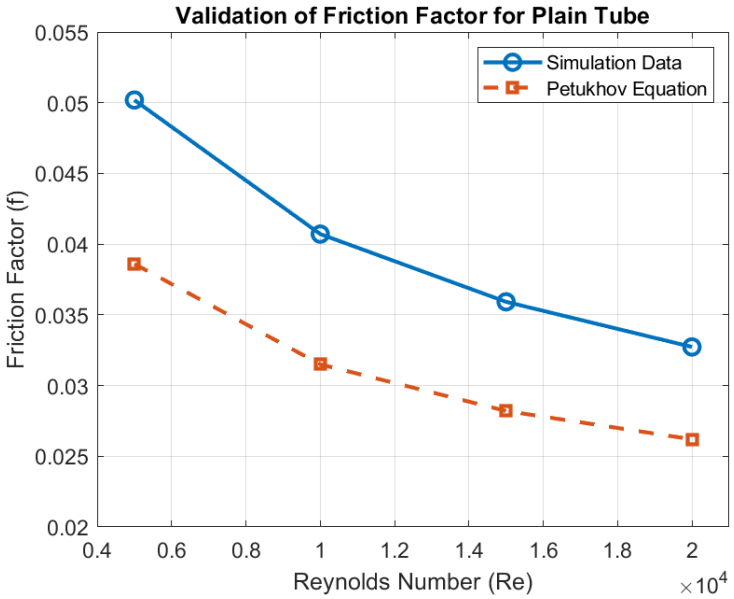


Fig. 9 Validation of the plain-tube friction factor against the Petukhov correlation

3.2 Thermophysical properties of Al_2O_3 nanofluid

The effective properties of the Al_2O_3 nanofluid, computed from Eqs. (4)–(7), are listed in Table 7. Increasing the Al_2O_3 volume fraction from 0.05% to 0.30% produced a small but consistent rise in thermal conductivity, density, and dynamic viscosity, while the specific heat decreased slightly a direct consequence

of the higher conductivity and density, but lower specific heat, of Al_2O_3 relative to water. Because these property changes are modest over the concentration range tested, their effect on the heat transfer and friction results (Sections 3.3–3.5) is correspondingly small compared with the effect of insert geometry.

Table 7. Thermophysical properties of Al_2O_3 nanofluid at the three volume fractions studied.

Working fluid	k (W/m·K)	Cp (J/kg·K)	ρ (kg/m³)	μ (Pa·s)
Base fluid + 0.05% Al_2O_3	0.6074	4175.93	998.85	9.00×10^{-4}
Base fluid + 0.15% Al_2O_3	0.6091	4162.41	1001.82	9.02×10^{-4}
Base fluid + 0.30% Al_2O_3	0.6118	4142.27	1006.28	9.06×10^{-4}

3.3 Effect of PTT inserts on Nusselt number

All three PTT configurations produced a substantially higher Nusselt number than the plain tube at every Reynolds number and nanofluid concentration tested, confirming that the swirl flow and additional flow disruption generated by the rectangular perforations enhance convective heat transfer beyond what the tape alone would achieve. Representative Nu–Re trends for φ = 0.05% are shown in Figs. 10–12 for PTT-01, PTT-02, and PTT-03, respectively; the trend is qualitatively similar at 0.15% and 0.30%. At Re = 20,000, the Nusselt number reached 211.6 (PTT-01), 214.8 (PTT-02), and 213.8 (PTT-03) at φ = 0.05% a 47–52% enhancement over the plain tube (Nu = 141.7). PTT-02, with the intermediate perforation size (10 mm × 20 mm), consistently gave the highest Nusselt number of the three geometries, indicating that this perforation size produces the most effective combination of swirl intensity and near-wall mixing. The effect of nanofluid concentration on Nusselt number was small and, counterintuitively, slightly negative the 0.05% case gave marginally higher Nu than 0.15% or 0.30% at a given Reynolds number, because the higher viscosity at greater loading slightly dampens the swirl induced mixing even as thermal conductivity rises.

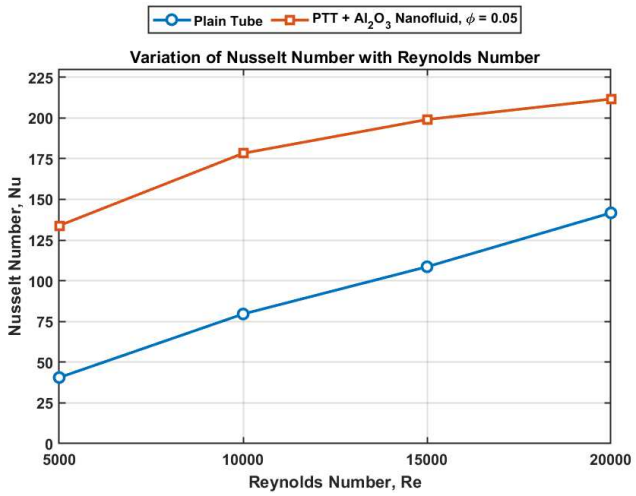


Fig. 10 Nusselt number versus Reynolds number for PTT-01 at φ = 0.05%

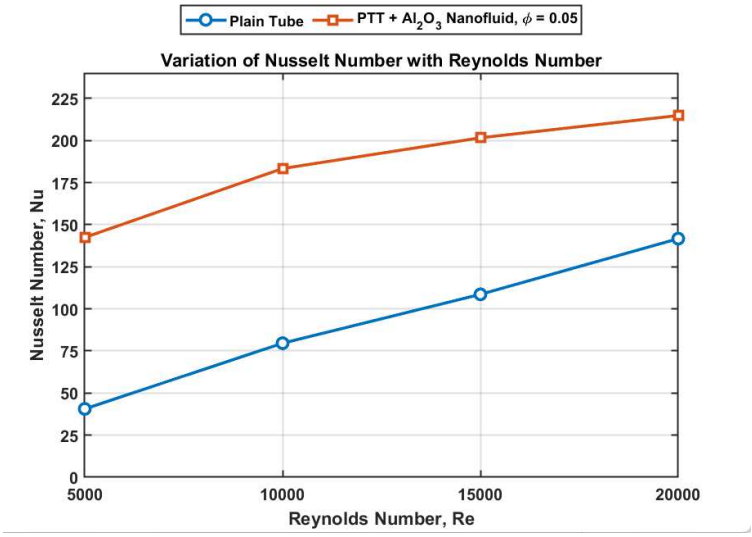


Fig. 11 Nusselt number versus Reynolds number for PTT-02 at φ = 0.05%

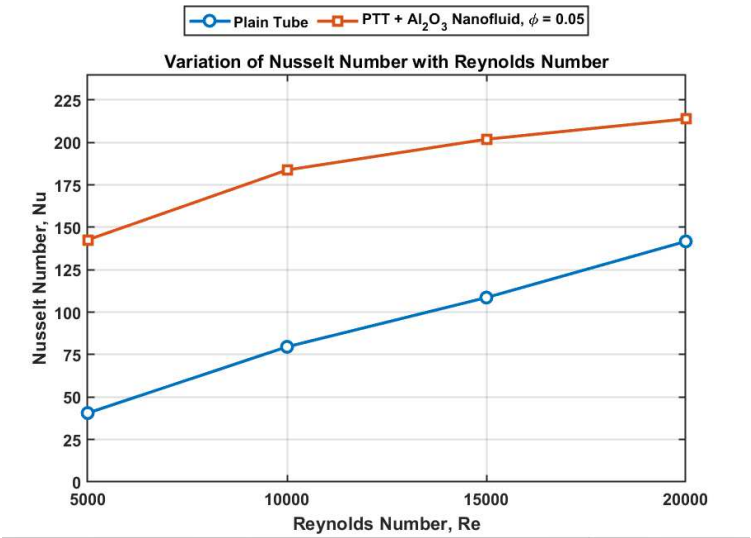


Fig. 12 Nusselt number versus Reynolds number for PTT-03 at φ = 0.05%

3.4 Effect of PTT inserts on friction factor

The friction factor decreased with Reynolds number for the plain tube and for all PTT configurations, as expected for turbulent flow, but the PTT inserted tubes showed a substantially higher friction factor than the plain tube at every condition owing to the additional flow blockage and swirl generated by the tape (Figs. 13–15). At Re = 20,000 and φ = 0.05%, the friction factor was 0.1850 (PTT-01), 0.2084 (PTT-02), and 0.2051 (PTT-03) 5.5 to 6.1 times the plain-tube value. PTT-02 produced the highest friction factor of the three geometries, mirroring its superior heat transfer performance: the same perforation size that maximizes swirl-driven mixing also maximizes flow resistance. The effect of Al_2O_3 concentration on friction factor was minor, with a slight increase at higher loading due to the corresponding rise in nanofluid viscosity.

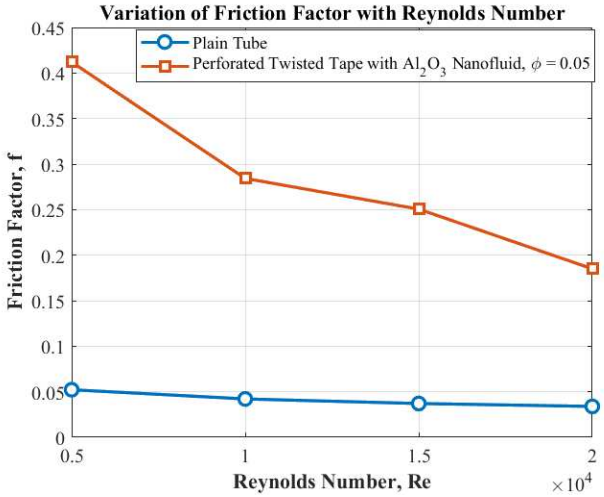


Fig. 13 Friction factor versus Reynolds number for PTT-01 at φ = 0.05%

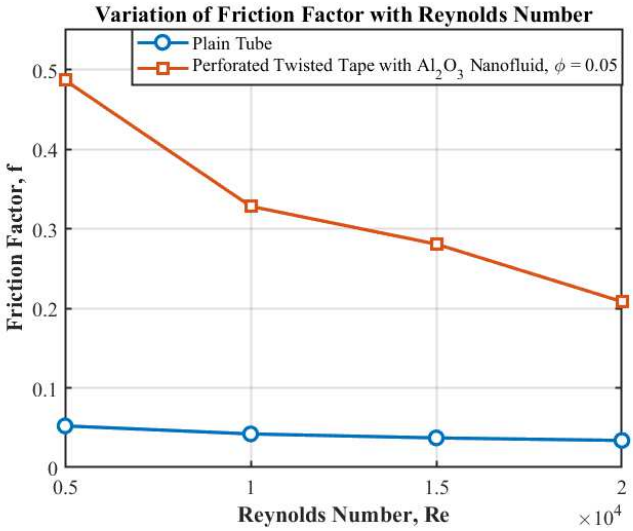


Fig. 14 Friction factor versus Reynolds number for PTT-02 at φ = 0.05%

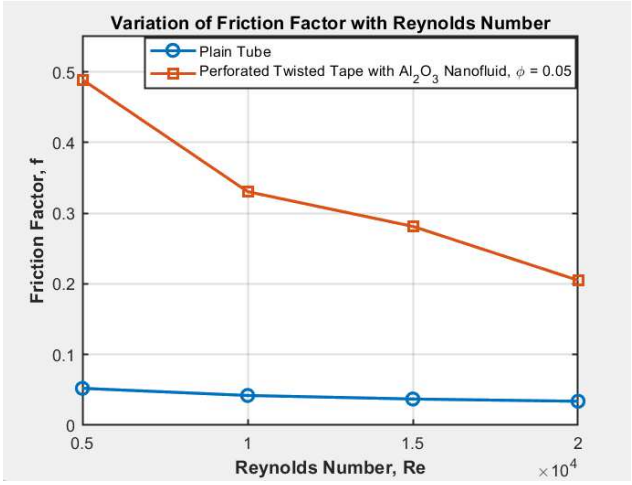


Fig. 15 Friction factor versus Reynolds number for PTT-03 at φ = 0.05%

3.5 Thermal enhancement efficiency

Because the Nusselt number gain from the PTT inserts is accompanied by a proportionally larger friction factor penalty, the overall benefit of each configuration was assessed through the thermal enhancement efficiency, η (Eq. 11), evaluated at Re = 20,000 where the Nusselt number enhancement is largest for each geometry. The results are summarized in Table 8 and Figs. 16-18. Although PTT-02 gave the highest Nusselt number ratio (1.52 at φ = 0.05%) of the three inserts, it also produced the highest friction factor ratio (6.15), so that its thermal enhancement efficiency (0.828) was lower than that of PTT-01. PTT-01 achieved the best overall balance, with η = 0.848 at φ = 0.05%, owing to its comparatively modest friction factor ratio (5.46) alongside a still-substantial Nusselt number ratio (1.49). PTT-03 fell between the two, with η ≈ 0.828. In all cases, η remained below unity, indicating that the frictional penalty of these rectangular-cut PTT inserts exceeds the corresponding heat transfer gain when compared on an equal-pumping-power basis; nevertheless, the values obtained are close to unity and comparable to those reported for other perforated tape designs in the literature. Increasing the Al_2O_3 volume fraction from 0.05% to 0.30% reduced η only marginally (by less than 0.5% across the concentration range for every insert), confirming that insert geometry rather than nanofluid loading is the dominant lever for thermal-hydraulic optimization in this system.

Table 8. Thermal enhancement efficiency of the PTT inserts with Al_2O_3 nanofluid at Re = 20,000.

Insert	φ (%)	Nu	Nu/Nu₀	f	f/f₀	(f/f₀)^1/3	η
PTT-01	0.05	211.59	1.4934	0.1850	5.4572	1.7606	0.8482
PTT-02	0.05	214.80	1.5161	0.2084	6.1486	1.8320	0.8276
PTT-03	0.05	213.81	1.5091	0.2051	6.0490	1.8221	0.8282
PTT-01	0.15	211.43	1.4922	0.1856	5.4742	1.7624	0.8467
PTT-02	0.15	214.65	1.5150	0.2089	6.1633	1.8335	0.8263
PTT-03	0.15	213.65	1.5080	0.2057	6.0677	1.8239	0.8268
PTT-01	0.30	211.20	1.4906	0.1863	5.4941	1.7645	0.8448
PTT-02	0.30	214.41	1.5133	0.2099	6.1910	1.8362	0.8242
PTT-03	0.30	213.41	1.5063	0.2065	6.0909	1.8263	0.8248

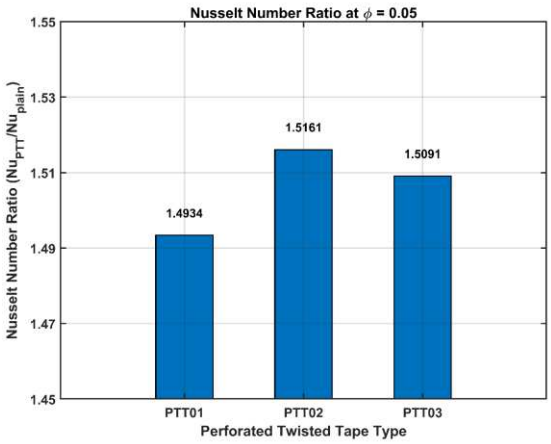


Fig. 16 Nusselt number ratio comparison for the PTT configurations at φ = 0.05%

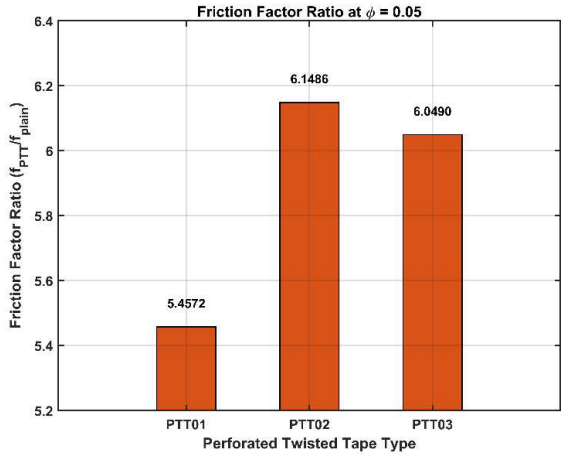


Fig. 17 Friction factor ratio comparison for the PTT configurations at φ = 0.05%

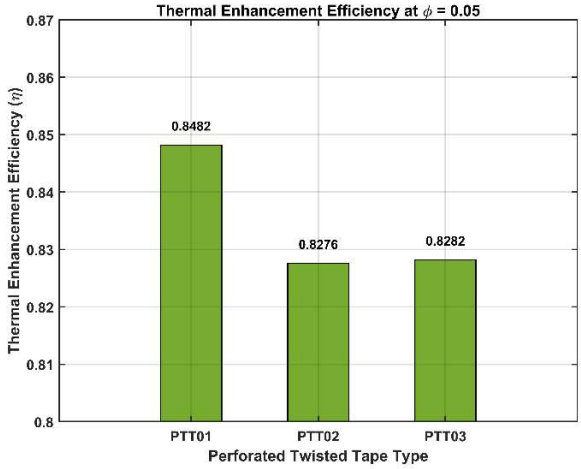


Fig. 18 Thermal enhancement efficiency comparison for the PTT configurations at φ = 0.05%

3.6 Qualitative flow and thermal-field analysis

Velocity streamlines confirm that the perforated twisted tape generates a sustained helical swirl along the full tube length (Fig. 19), which continuously redirects flow between the tube core and the near-wall region and disrupts the thermal boundary layer responsible for the Nusselt number enhancement reported above. Outlet temperature contours (Fig. 20) become progressively more uniform as the Reynolds number increases, reflecting the improved cross-sectional mixing produced by the swirling flow at higher flow rates. Temperature contours at Re = 20,000 (Fig. 21) show a more uniform thermal field as the Al_2O_3 volume fraction increases, consistent with the higher effective thermal conductivity of the nanofluid. Velocity contours (Fig. 22) show the characteristic asymmetric, swirl-dominated velocity field imposed by the tape, while pressure contours (Fig. 23) show a continuous pressure decay along the flow direction, illustrating the hydraulic penalty that accompanies the swirl-enhanced mixing.

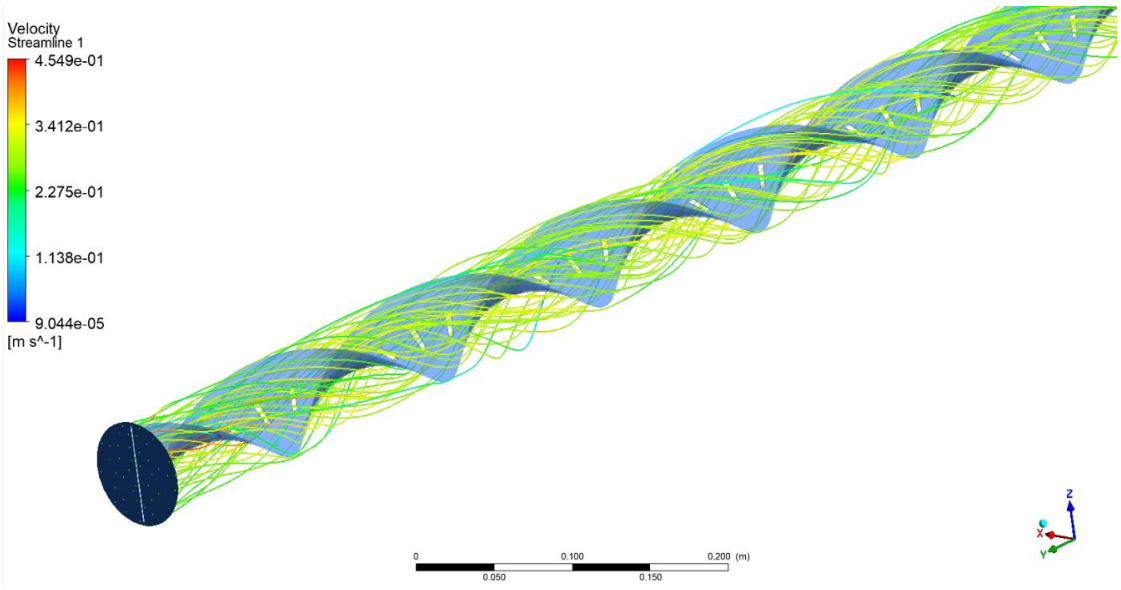


Fig. 19 Velocity streamline distribution in the tube fitted with the perforated twisted tape insert

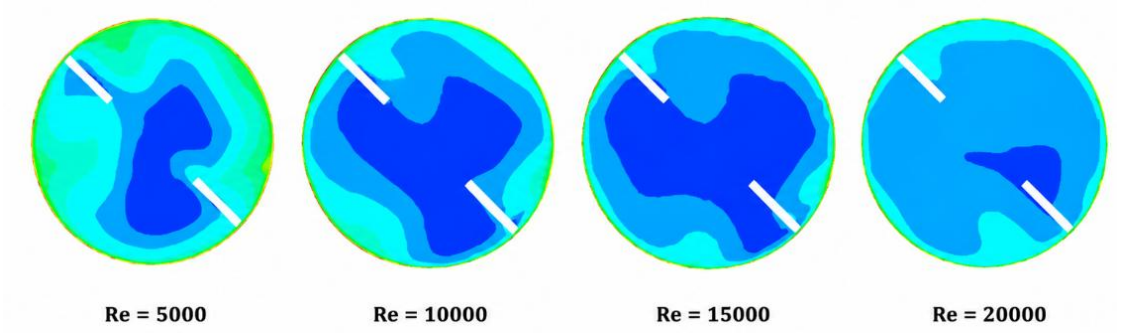


Fig. 20 Outlet temperature contours of PTT-01 with Al_2O_3 nanofluid (φ = 0.05%) at Re = 5000, 10000, 15000, and 20000

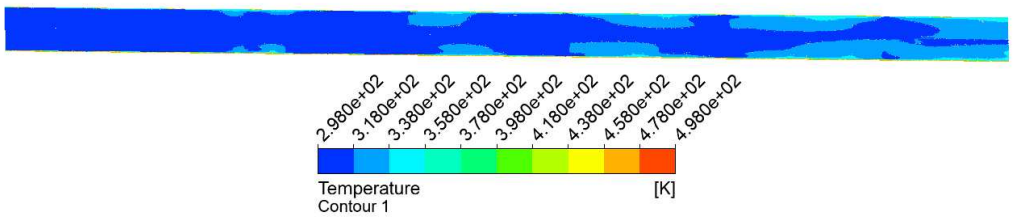


Fig. 21 Temperature contours of PTT-01 at Re = 20,000 for φ = 0.05%

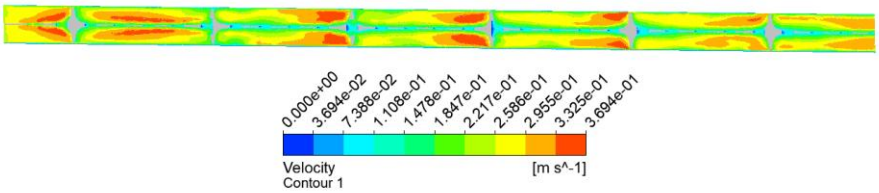


Fig. 22 Velocity contour of PTT-01 (φ = 0.05%, Re = 20,000)

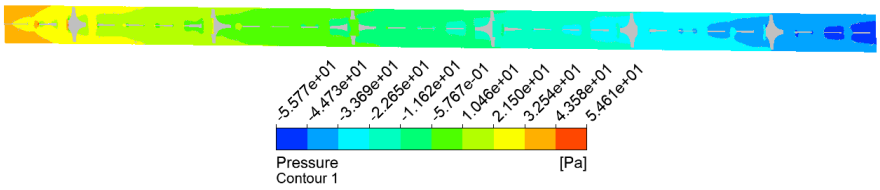


Fig. 23 Pressure contour of PTT-01 (φ = 0.05%, Re = 20,000)

4 Conclusions

A CFD investigation of rectangular-cut perforated twisted tape (PTT) inserts combined with Al_2O_3 nanofluid was carried out in a circular tube heat exchanger under constant heat flux, over Re = 5000–20,000 and φ = 0.05–0.30%. The following conclusions are drawn:

1. All three PTT geometries substantially increased the Nusselt number relative to the plain tube (47–52% at Re = 20,000), through swirl generation and disruption of the thermal boundary layer, but this was accompanied by a 5.5- to 6.1-fold increase in friction factor.
2. PTT-02 (10 mm × 20 mm perforation) produced the strongest heat transfer enhancement of the three geometries but also the highest hydraulic penalty; PTT-01 (20 mm × 30 mm) gave the best overall thermal enhancement efficiency (η = 0.848 at φ = 0.05%, Re = 20,000).
3. The thermal enhancement efficiency remained below unity for all configurations tested, indicating that, on an equal-pumping-power basis, the frictional penalty of these inserts slightly exceeds the heat transfer gain; insert geometry should therefore be selected according to the application's tolerance for pressure drop rather than by maximizing Nusselt number alone.
4. Al_2O_3 nanoparticle loading had a comparatively minor effect on both Nusselt number and friction factor over the 0.05–0.30% range, changing the thermal enhancement efficiency by less than 0.5%; insert geometry, not nanofluid concentration, is the dominant design variable in this system.
5. Qualitative streamline, temperature, velocity, and pressure contours confirmed that the PTT inserts sustain a continuous helical swirl that improves cross-sectional thermal mixing at the cost of a continuous pressure decay along the tube.

Future work should extend this analysis to hybrid nanofluids, a wider range of nanoparticle concentrations, and additional perforation shapes, to identify configurations that push the thermal enhancement efficiency above unity.

References

[1] E. Tavousi, N. Perera, D. Flynn, R. Hasan, Heat transfer and fluid flow characteristics of the passive method in double tube heat exchangers : A critical review, Int. J. Thermofluids 17 (2027) 100282. https://doi.org/10.1016/j.ijft.2023.100282.

[2] M. Omidi, M. Farhadi, M. Jafari, Omidi, Mohamad, Mousa Farhadi, and Mohamad Jafari. “A comprehensive review on double pipe heat exchangers.” Applied Thermal Engineering 110 (2017): 1075-1090., 110 (2017) 1075–1090.

[3] T. Rahman, K. Habib, N. Quader, N. Aslfattahi, Heliyon Effect of porous density of twisted tape inserts on heat transfer performance inside a closed conduit, Heliyon 9 (2023) e21206. https://doi.org/10.1016/j.heliyon.2023.e21206.

[4] O.W. Abass, M. Tekir, Numerical investigation on effects of plain , perforated , and dimpled twisted tape inserts in a tube to flow and heat transfer characteristics, Numer. Heat Transf. Part A Appl. 86 (2025) 6650–6669. https://doi.org/10.1080/10407782.2024.2377705.

[5] A.J. Abdulhamed, A. Al-akam, W.J. Khudhayer, A.S. Allw, Tubular Heat Enhancement Using Twisted Tape Inserts with Large Holes, (2024). https://doi.org/10.32604/ee.2023.045583.

[6] H. Bucak, F. Yılmaz, Chemical Engineering & Processing : Process Intensification The current state on the thermal performance of twisted tapes : A geometrical categorisation approach, Chem. Eng. Process. Process Intensif. 153 (2020) 107929. https://doi.org/10.1016/j.cep.2020.107929.

[7] J. Yang, Z. Feng, Heliyon Assessing the use of PEC and jf methods for strengthening the evaluation of new heat exchangers, Heliyon 10 (2024) e30869. https://doi.org/10.1016/j.heliyon.2024.e30869.

[8] H. Maddah, M. Alizadeh, N. Ghasemi, S. Rafidah, W. Alwi, International Journal of Heat and Mass Transfer Experimental study of Al 2 O 3 / water nanofluid turbulent heat transfer enhancement in the horizontal double pipes fitted with modified twisted tapes, HEAT MASS Transf. 78 (2014) 1042–1054. https://doi.org/10.1016/j.ijheatmasstransfer.2014.07.059.

[9] L.S. Sundar, K. V Sharma, International Journal of Heat and Mass Transfer Turbulent heat transfer and friction factor of Al 2 O 3 Nanofluid in circular tube with twisted tape inserts, Int. J. Heat Mass Transf. 53 (2010) 1409–1416. https://doi.org/10.1016/j.ijheatmasstransfer.2009.12.016.

[10] H.M.S. Murthy, R.N. Hegde, N. Rai, Effect on performance of a CTHE by using twisted tapes and Al 2 O 3 nanofluids : an experimental study and correlation development, Sādhanā 0123456789 (2024). https://doi.org/10.1007/s12046-024-02557-1.

[11] C.T. Tape, Performances of SiC / Water and Al 2 O 3 / Water, (2020).

[12] H.K. Pazarlıoğlu, M. Gürdal, M. Tekir, K. Arslan, IMPACT OF TWISTED DUCTS WITH DIFFERENT TWIST RATIOS ON HEAT TRANSFER AND FLUID CHARACTERISTICS OF NiO / WATER NANOFLUID FLOW UNDER MAGNETIC FIELD EFFECT, 53 (2022) 55–71.

[13] M.E. Nakhchi, J.A. Esfahani, Numerical investigation of rectangular-cut twisted tape insert on performance improvement of heat exchangers, Int. J. Therm. Sci. 138 (2019) 75–83. https://doi.org/10.1016/j.ijthermalsci.2018.12.039.

[14] A.E. Almerane, Effect of Thickness on Thermo-Hydraulic Performance of a DPHE with Twisted Perforated Tapes : A Numerical Study, (2026) 1–30.

Statements and Declarations

Funding

No funding was received for conducting this study or preparing this manuscript.

Competing interests

The authors declare that they have no competing interests.

Data availability

The data supporting the findings of this study are available from the corresponding author on reasonable request.

Author contributions

Sajid Akram Bhuiyan: Conceptualization, Methodology, Software, Investigation, Data curation, Formal analysis, Visualization, Writing - original draft.
MM Roshid: Conceptualization, Methodology, Supervision.
Mohammad Fahim Ahmed: Formal analysis, Writing - review and editing, Software, Investigation.
Md. Suez: Formal analysis, Writing - review and editing.

Ethics approval

Not applicable. This study reports computational fluid-dynamics simulations and did not involve human participants or animals.

Consent to participate

Not applicable.

Consent for publication

Not applicable.